Nonreciprocal optical response of helical periodic structures of plasma spheres in a static magnetic field

A. Christofi* and N. Stefanou

Department of Solid State Physics, University of Athens, Panepistimioupolis, GR-157 84 Athens, Greece

(Received 28 January 2013; published 20 March 2013)

A detailed and rigorous theoretical investigation of the optical properties of a generic three-dimensional chiral structure of plasma spheres, without and under the action of an external static uniform magnetic field, is presented. Corresponding photonic band diagrams in conjunction with relevant transmission spectra, calculated by the full electrodynamic layer-multiple-scattering method properly extended to the case of gyrotropic spherical scatterers, are discussed in the light of the theory of nonsymmorphic space groups. This analysis provides a consistent interpretation of some remarkable features and effects like Dirac points, polarization-dependent transmission, as well as band splitting and non-reciprocal optical response that emerge as a result of time-reversal-symmetry breaking, induced by the external static magnetic field, and the lack of space-inversion symmetry in the crystal.

DOI: 10.1103/PhysRevB.87.115125 PACS number(s): 42.70.Qs, 81.05.Xj, 41.20.Jb, 42.25.Bs

I. INTRODUCTION

The electromagnetic (EM) properties of a medium can be efficiently manipulated by periodic structuring on a length scale comparable to the corresponding wavelength, thus offering impressive possibilities for tailoring the light-matter interaction. In recent years, considerable effort has been devoted to the investigation of so-called magnetophotonic crystals. These are macroscopic structures in which the EM response of at least one of the constitutive building units can be controlled by a static magnetic field and exhibit very interesting properties. For example, it has been established that, in such composites media, strong photon confinement in the vicinity of magnetically active components results in large enhancement of linear and nonlinear magneto-optical effects (see Ref. 1 and references therein). On the other hand, the influence of a static magnetic field on light propagation in random media and consequent phenomena, which mirror corresponding effects for charge transport in a magnetic field, has also been studied both experimentally and theoretically (see Ref. 2 and references therein).

The gyrotropic response of materials, induced by a static uniform magnetic field (the Faraday effect) oriented along, say, the z direction, is described by a relative electric permittivity and/or magnetic permeability tensor of the form

$$\overleftrightarrow{\epsilon}_g = \begin{pmatrix} \epsilon_r & -i\epsilon_\kappa & 0 \\ i\epsilon_\kappa & \epsilon_r & 0 \\ 0 & 0 & \epsilon_z \end{pmatrix}, \quad \overleftrightarrow{\mu}_g = \begin{pmatrix} \mu_r & -i\mu_\kappa & 0 \\ i\mu_\kappa & \mu_r & 0 \\ 0 & 0 & \mu_z \end{pmatrix}. \qquad (1)$$

Because of the lack of local time-reversal symmetry, gyrotropic materials are ideally suited for designing nonreciprocal photonic devices,[3,4] which are of crucial importance in optical communication and computing technologies because of their ability to eliminate crosstalk and feedback. Spectral nonreciprocity is in principle encountered in systems which lack both time-reversal and space-inversion symmetries,[5] such as magnetophotonic structures without an inversion center, and various designs have been proposed and elaborated for this purpose.[6–11] Moreover, there has been considerable interest in the occurrence of topologically nontrivial photonic modes, such as chiral edge states, in appropriately designed magnetophotonic structures,[12–22] which allow for reflection-free transport of light even in the presence of strong disorder.

In the present paper we report a thorough theoretical investigation of the optical properties of a generic three-dimensional chiral photonic crystal consisting of plasma spheres in a helical arrangement, and we study, in particular, the effect of an external static uniform magnetic field by means of full electrodynamic calculations using the layer-multiple-scattering method[23,24] properly extended to the case of gyrotropic spherical scatterers. A comprehensive analysis of calculated photonic band diagrams in conjunction with corresponding transmission spectra, in the light of the theory of nonsymmorphic space groups, clarifies the origin of some remarkable features and effects like Dirac points, polarization-dependent transmission, band splitting, and nonreciprocal optical response, to a degree that goes beyond existing interpretation.

II. DESCRIPTION OF THE CRYSTAL

We consider a tetragonal crystal defined by the primitive lattice vectors $\mathbf{a}_1 = (a,0,0)$, $\mathbf{a}_2 = (0,a,0)$, and $\mathbf{a}_3 = (0,0,d)$ and a basis of four plasma spheres, of radius S, centered at $(0,0,0)$, $(b,0,d/4)$, $(b,b,d/2)$, and $(0,b,3d/4)$, as shown in Fig. 1, embedded in a homogeneous host medium of relative electric permittivity $\epsilon = 1$ and magnetic permeability $\mu = 1$. This chiral crystal structure, originally proposed with dielectric spheres as an artificial optically active material,[25] was later investigated with plasma spheres in relation to the occurrence of negative-slope photonic bands,[26] and a Dirac point in the photonic band structure was identified at the center of the first Brillouin zone.[27] Today, such structures can be realized in the laboratory using modern nanofabrication methods like lithography[28,29] and directed assembly,[30,31] and, recently, the potential of the DNA origami approach for the programmable and nanometer-precise design of helical assemblies of metallic nanoparticles was also demonstrated.[32,33]

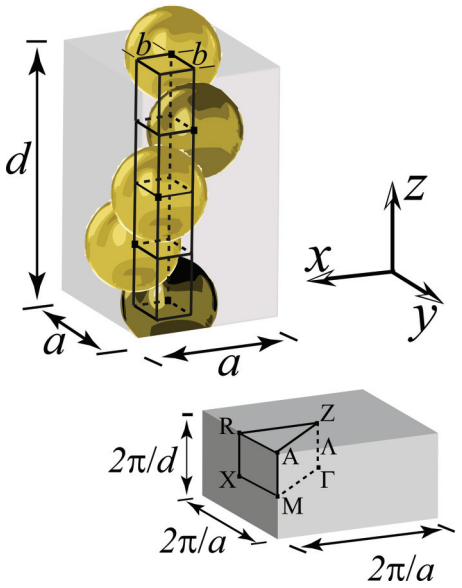

FIG. 1. (Color online) The unit cell of the crystal under consideration: A tetragonal lattice with a basis of four plasma spheres described by the Drude relative electric permittivity of Eq. (2), of radius $S = 0.2c/\omega_p$, in a helical arrangement along the z direction ($a = c/\omega_p$, $d = 2c/\omega_p$,$b = 0.3c/\omega_p$) and the corresponding first Brillouin zone.

We assume that the plasma spheres are described by a relative magnetic permeability $\mu_p = 1$ and by the simple yet effective Drude relative electric permittivity:[34]

$$\epsilon_p = 1 - \frac{\omega_p^2}{\omega(\omega + i/\tau)}, \tag{2}$$

where τ is the relaxation time of the free carriers and ω_p is the bulk plasma frequency: $\omega_p^2 = ne^2/(m\epsilon_0)$, with ϵ_0 being the vacuum permittivity and n, $-e$, and m being the carrier density, charge, and mass, respectively, which naturally introduces c/ω_p as the length unit, c being the velocity of light in vacuum. We note that, assuming $\hbar\omega_p \simeq 10$ eV, which is a typical value for metals, c/ω_p corresponds to about 20 nm. For semiconductors, on the other hand, as their carrier densities can be easily varied within a broad range of values, which are much lower than those in metals, the plasma frequency is much smaller (typically at mid- and far-infrared frequencies) and the length unit c/ω_p increases accordingly. For the crystal under consideration, we take $a = c/\omega_p$, $d = 2c/\omega_p$, $S = 0.2c/\omega_p$, and $b = 0.3c/\omega_p$.

In the presence of a static uniform magnetic field $\mathbf{B}$, the response of a plasma to a time-harmonic EM wave of angular frequency ω, with electric-field component $\mathbf{E} = \mathbf{E}_0 \exp(-i\omega t)$, is described by the equation of motion of the electrons: $m\ddot{\mathbf{r}} = -m\tau^{-1}\dot{\mathbf{r}} - e\mathbf{E} - e\dot{\mathbf{r}} \times \mathbf{B}$. The resulting polarization density, $\mathbf{P} = -ne\mathbf{r}$, defines an electric displacement vector $\mathbf{D} = \epsilon_0\mathbf{E} + \mathbf{P}$ and finally yields the relative electric permittivity tensor $\overleftrightarrow{\epsilon_g}$ of the magnetized plasma through $\mathbf{D} = \epsilon_0 \overleftrightarrow{\epsilon_g}\mathbf{E}$. Defining the cyclotron resonance frequency, $\omega_c = eB/m$, if $\mathbf{B}$ is oriented along the z direction, after some straightforward algebra we find that $\overleftrightarrow{\epsilon_g}$ has the gyrotropic form given by Eq. (1) with

$$\begin{aligned} \epsilon_r &= 1 - \frac{\omega_p^2[1 + i/(\tau\omega)]}{(\omega + i/\tau)^2 - \omega_c^2}, \\ \epsilon_z &= 1 - \frac{\omega_p^2}{\omega(\omega + i/\tau)}, \\ \epsilon_\kappa &= -\frac{\omega_c}{\omega}\frac{\omega_p^2}{(\omega + i/\tau)^2 - \omega_c^2}. \end{aligned} \tag{3}$$

We note that, by setting $\omega_c = 0$, $\overleftrightarrow{\epsilon_g}$ becomes a diagonal tensor with all of its diagonal elements equal to ϵ_p given by Eq. (2), as expected. In our calculations we shall neglect dissipative losses ($\tau^{-1} = 0$) in order to ensure an unambiguous interpretation of the photonic band structure.

III. METHOD OF CALCULATION

We study the optical properties of the crystal under consideration, without and under the action of the static magnetic field, by means of rigorous full electrodynamic calculations using the layer-multiple-scattering method,[23,24] properly extended to the case of gyrotropic spherical scatterers.[35] In this method, the properties of the individual scatterers enter only through the corresponding T matrix. The EM field at a given frequency is expanded into proper vector spherical waves, inside and outside the scatterer, and the T matrix is obtained by matching the appropriate boundary conditions at the surface of the scatterer. In a gyrotropic sphere, the multipole expansion involves vector spherical waves of different wave numbers. These wave numbers and the corresponding EM field expansion coefficients are given by the eigenvalues and eigenvectors of a matrix, which involves only the elements of the corresponding relative electric permittivity (and/or magnetic permeability) tensor and angular momentum numbers. Following this approach, which has been elaborated by different authors,[36–39] we finally obtain a nondiagonal scattering T matrix in the given spherical-wave representation from a set of coupled linear equations that relate the expansion coefficients of the scattered field to those of the incident field.

Within the layer-multiple-scattering method, we view a three-dimensional crystal as a sequence of layers of scatterers parallel to the x–y plane. The layers must have the same two-dimensional periodicity, while periodicity in the z direction is not a prerequisite. At a first step, in-plane multiple scattering is evaluated in the given spherical-wave basis using the T matrix of the individual scatterers and proper propagator functions. Subsequently, interlayer scattering is calculated in a plane-wave basis through appropriate transmission and reflection matrices, by including all propagating and evanescent components of the wave field necessary to obtain convergence. In this way, interaction between the scatterers is fully taken into account. Truncating the spherical-wave expansions at $l_{\max} = 3$ and taking into account 37 two-dimensional reciprocal-lattice vectors in the relevant plane-wave expansions,[23,24] we ensure good convergence in our calculations for the structure under consideration.

The scattering S matrix of a multilayer slab, which transforms the incident into the outgoing wave field, is obtained by combining the transmission and reflection matrices of the

component layers. The ratio of the transmitted or reflected energy flux to the energy flux associated with the incident wave defines the transmittance or reflectance of the slab, respectively. On the other hand, for a three-dimensional crystal consisting of an infinite periodic sequence of layers, stacked along the z direction, applying the Bloch theorem for the wave field in the region between two consecutive unit slices leads to an eigenvalue equation, which gives the z component of the Bloch wave vector, k_z, for the given angular frequency ω and in-plane wave-vector component reduced within the surface Brillouin zone, $\mathbf{k}_\parallel$, which are conserved quantities in the scattering process. The eigenvalues $k_z(\omega,\mathbf{k}_\parallel)$, looked upon as functions of real ω, define, for each $\mathbf{k}_\parallel$, lines in the complex k_z plane. Taken together they constitute the complex band structure of the infinite crystal associated with the given crystallographic plane. A line of given $\mathbf{k}_\parallel$ may be real (in the sense that k_z is real) over certain frequency regions and be complex (in the sense that k_z is complex) for ω outside these regions. It turns out that, for given $\mathbf{k}_\parallel$ and ω, out of the eigenvalues $k_z(\omega,\mathbf{k}_\parallel)$, none or, at best, a few are real and the corresponding eigenvectors represent propagating modes of the EM field in the given infinite crystal. The remaining eigenvalues $k_z(\omega,\mathbf{k}_\parallel)$ are complex, and the corresponding eigenvectors represent evanescent waves. These have amplitudes which increase exponentially in the positive or negative z direction and, unlike the propagating waves, do not exist as physical entities in the infinite crystal. However, they are an essential part of the physical solutions of the EM field in a slab of finite thickness. A region of frequency where propagating waves do not exist, for given $\mathbf{k}_\parallel$, constitutes a frequency gap of the EM field for the given $\mathbf{k}_\parallel$. If over a frequency region no propagating wave exists whatever the value of $\mathbf{k}_\parallel$, then this region constitutes an absolute frequency gap.

IV. RESULTS AND DISCUSSION

To begin with, we summarize the main features of the photonic band structure of the crystal under study, in the absence of a static magnetic field. As shown in Fig. 2, along the [001] direction, at low frequencies (below $\omega \approx 0.55\omega_p$) we obtain two nondegenerate extended bands, so close to each other that they are indistinguishable at the scale of the figure, associated with propagation in a homogeneous effective medium. At higher frequencies, the dispersion diagram is characterized by the presence of narrow bands, which originate from the dipole particle-plasmon modes of the individual spheres, at $\omega_1 = 0.575\omega_p$, weakly interacting between them, and hybridize with the extended bands giving rise to frequency gaps. We note that the total number of these narrow bands, which are displayed in an enlarged view in the margin of Fig. 2, is 12, as expected from the threefold degeneracy of the dipole particle-plasmon modes of the sphere and the number of spheres per unit cell ($12 = 3 \times 4$). Narrow bands stemming from higher multipole particle-plasmon modes are above the frequency region under consideration. It is worth noting that, though the crystal under study does not posses space-inversion symmetry, the symmetry $\omega(\mathbf{k}) = \omega(-\mathbf{k})$ persists because of time-reversal symmetry.

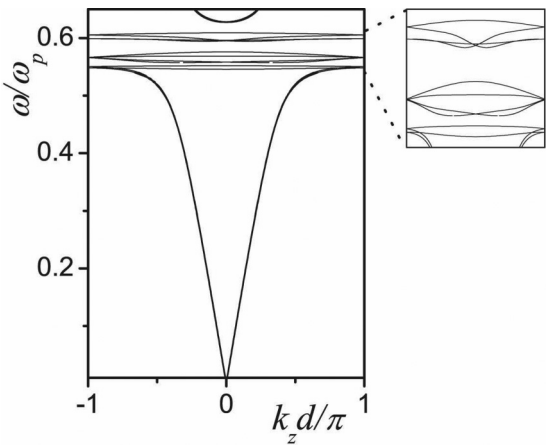

FIG. 2. Photonic band structure of the crystal of Fig. 1 along its [001] direction, in the absence of a static magnetic field. An enlarged view of the dispersion diagram in the frequency region of the narrow bands is displayed in the margin.

A rigorous and consistent analysis of the symmetry properties of the photonic band structure of Fig. 2, which goes beyond existing interpretation, is provided by the theory of nonsymmorphic space groups. In the absence of a static magnetic field, the crystal of Fig. 1 remains invariant under the operations of the nonsymmorphic space group D_4^7, described in the Appendix. Along the Λ direction, i.e., for $\mathbf{k} = (0,0,k_z)$ (see Fig. 1) the frequency bands have the symmetry of the irreducible representations of the relevant factor group, $\mathcal{G}(\mathbf{k})/\mathcal{T}(\mathbf{k})$ (see Table I), and not of a fixed point group as in the case of symmorphic space groups.[40,41] The bands along this direction are nondegenerate since all the irreducible representations of the factor group of Table I are one dimensional. Moreover, none of these bands corresponds to purely left- or right-circularly polarized (LCP and RCP, respectively) Bloch modes because no irreducible representation of this factor group has LCP and RCP basis functions. There is a different degree of LCP and RCP admixture that varies along a specific band, as presented by the color scale in Fig. 3 that shows the projection of the corresponding eigenvector onto the basis spanned by the LCP and RCP states. It is also interesting to note that the correspondence between the irreducible representations—$\Lambda_{1(\phi)} \to \Lambda_{4(\phi-\pi)}$, $\Lambda_{2(\phi)} \to \Lambda_{3(\phi-\pi)}$, $\Lambda_{3(\phi)} \to \Lambda_{1(\phi-\pi)}$, $\Lambda_{4(\phi)} \to \Lambda_{2(\phi-\pi)}$, which can be easily established from Table I—accounts for the invariance of Bloch modes that differ by a reciprocal-lattice vector in the present case, i.e., by $(0,0,2\pi n/d)$, $n = 0,\pm1,\pm2,\ldots$, as requested (see Fig. 3). At the center Γ of the first Brillouin zone, i.e., for $\mathbf{k} = (0,0,0)$, the relevant factor group is isomorphic to the point group D_4 (see Table II). Compatibility between the irreducible representations of D_4 and of the factor group of Table I, for

TABLE I. Character table of the factor group $\mathcal{G}(\mathbf{k})/\mathcal{T}(\mathbf{k})$ for $\mathbf{k}$ on the axis Λ [$\mathbf{k} = (0,0,k_z)$] for the space groups D_4^7 and C_4^4 [$w_1 = \exp(-i\phi)$, $w_2 = \exp(i\phi/2)$ with $\phi = k_z d/2$].

	$\Lambda_{1(\phi)}$	$\Lambda_{2(\phi)}$	$\Lambda_{3(\phi)}$	$\Lambda_{4(\phi)}$
$\{\widehat{E}\|\mathbf{0}\}\mathcal{T}(\mathbf{k})$	1	1	1	1
$\{\widehat{C}_{2z}\|2\boldsymbol{\tau}\}\mathcal{T}(\mathbf{k})$	w_1	w_1	$-w_1$	$-w_1$
$\{\widehat{C}_{4z}\|\boldsymbol{\tau}\}\mathcal{T}(\mathbf{k})$	w_2^*	$-w_2^*$	iw_2^*	$-iw_2^*$
$\{\widehat{C}_{4z}^{-1}\|-\boldsymbol{\tau}\}\mathcal{T}(\mathbf{k})$	w_2	$-w_2$	$-iw_2$	iw_2

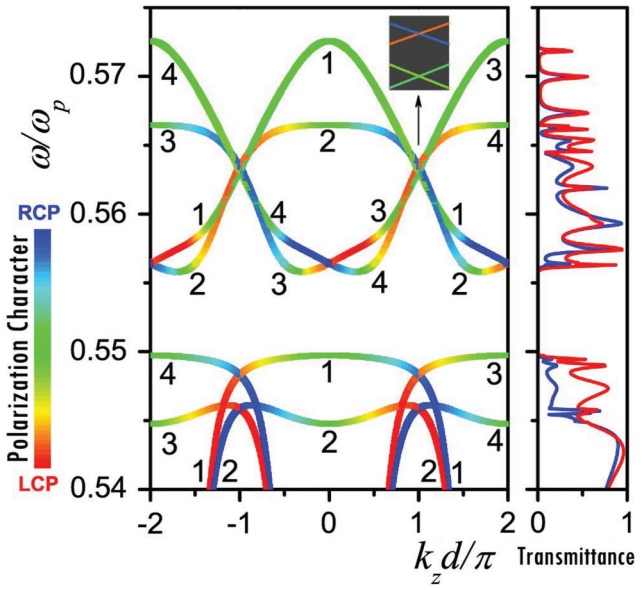

FIG. 3. (Color online) Photonic band structure of the crystal of Fig. 1 along its [001] direction, in the absence of a static magnetic field, in the frequency region about the lowest flat bands. The different bands are labeled by the index of the relevant irreducible representation of the appropriate factor group $\mathcal{G}(\mathbf{k})/\mathcal{T}(\mathbf{k})$ for $\mathbf{k} = (0,0,k_z)$ (see Table I). Inset: Enlarged view of the dispersion diagram in the region about the crossing points indicated by the arrow. Next to the band diagram we depict corresponding transmission spectra for LCP and RCP light incident normally on a (001) slab of the crystal consisting of 16 layers of spheres.

$\phi = 0$, implies that the bands of $\Lambda_{3(\phi)}$ and $\Lambda_{4(\phi)}$ symmetry along the Λ direction converge to a doubly degenerate point of E symmetry at the center of the first Brillouin zone. This is indeed observed in Fig. 3, at $\omega = 0.557\omega_p$, where two such bands cross linearly at the Dirac point identified by Yannopapas.[27] At the Z point, i.e., for $\mathbf{k} = (0,0,\pm\pi/d)$, all the permissible irreducible representations of the relevant factor group are two dimensional (see Table III), and this explains the fact that at this zone boundary all bands are paired and sticking together, giving rise to additional Dirac points as shown in Fig. 3. Compatibility between the permissible irreducible representations of the factor group associated with point Z and those of the factor group associated with the direction Λ, for $\phi = \pi/2$, implies that the bands of $\Lambda_{1(\phi)}$ and $\Lambda_{3(\phi)}$ symmetry converge to a doubly degenerate mode of Z_a symmetry and the bands of $\Lambda_{2(\phi)}$ and $\Lambda_{4(\phi)}$ symmetry converge to a doubly degenerate mode of Z_b symmetry at $\mathbf{k} = (0,0,\pi/d)$. Correspondingly, the bands of $\Lambda_{1(\phi)}$ and $\Lambda_{4(\phi)}$ symmetry converge to a doubly degenerate mode of

TABLE II. Character table of the point group D_4.

	A_1	B_1	A_2	B_2	E
$\widehat{E}$	1	1	1	1	2
$\widehat{C}_{2z}$	1	1	1	1	−2
$\widehat{C}_{4z}, \widehat{C}_{4z}^{-1}$	1	−1	1	−1	0
$\widehat{C}_{2x}, \widehat{C}_{2y}$	1	1	−1	−1	0
$\widehat{C}_{2a}, \widehat{C}_{2b}$	1	−1	−1	1	0

TABLE III. Characters of the permissible irreducible representations of the factor group $\mathcal{G}(\mathbf{k})/\mathcal{T}(\mathbf{k})$ at the point Z [$\mathbf{k} = (0,0,\pm\pi/d)$] for the space group D_4^7.

	Z_a	Z_b
$\{\widehat{E}\|\mathbf{0}\}\mathcal{T}(\mathbf{k})$	2	2
$\{\widehat{E}\|4\boldsymbol{\tau}\}\mathcal{T}(\mathbf{k})$	−2	−2
$\{\widehat{C}_{4z}\|\boldsymbol{\tau}\}\mathcal{T}(\mathbf{k}), \{\widehat{C}_{4z}^{-1}\|-\boldsymbol{\tau}\}\mathcal{T}(\mathbf{k})$	$\sqrt{2}$	$-\sqrt{2}$
$\{\widehat{C}_{4z}\|-3\boldsymbol{\tau}\}\mathcal{T}(\mathbf{k}), \{\widehat{C}_{4z}^{-1}\|3\boldsymbol{\tau}\}\mathcal{T}(\mathbf{k})$	$-\sqrt{2}$	$\sqrt{2}$
$\{\widehat{C}_{2z}\|2\boldsymbol{\tau}\}\mathcal{T}(\mathbf{k}), \{\widehat{C}_{2z}\|-2\boldsymbol{\tau}\}\mathcal{T}(\mathbf{k})$	0	0
$\{\widehat{C}_{2x}\|2\boldsymbol{\tau}\}\mathcal{T}(\mathbf{k}), \{\widehat{C}_{2y}\|4\boldsymbol{\tau}\}\mathcal{T}(\mathbf{k}),$ $\{\widehat{C}_{2x}\|-2\boldsymbol{\tau}\}\mathcal{T}(\mathbf{k}), \{\widehat{C}_{2y}\|\mathbf{0}\}\mathcal{T}(\mathbf{k})$	0	0
$\{\widehat{C}_{2a}\|\boldsymbol{\tau}\}\mathcal{T}(\mathbf{k}), \{\widehat{C}_{2a}\|-3\boldsymbol{\tau}\}\mathcal{T}(\mathbf{k}),$ $\{\widehat{C}_{2b}\|-\boldsymbol{\tau}\}\mathcal{T}(\mathbf{k}), \{\widehat{C}_{2b}\|3\boldsymbol{\tau}\}\mathcal{T}(\mathbf{k})$	0	0

Z_a symmetry and the bands of $\Lambda_{2(\phi)}$ and $\Lambda_{3(\phi)}$ symmetry converge to a doubly degenerate mode of Z_b symmetry at $\mathbf{k} = (0,0,-\pi/d)$, as shown in Fig. 3.

In Fig. 3, next to the band diagram, we depict corresponding transmission spectra for LCP and RCP light incident normally on a (001) slab of the crystal consisting of 16 layers of spheres. The characterization of the band eigenmodes by their degree of LCP and RCP admixture allows for a consistent interpretation of the transmission spectra. In the frequency region extending from $0.546\omega_p$ to $0.549\omega_p$, we can see that the modes with positive group velocity have a predominant LCP character and thus they couple predominantly to a plane EM wave with the same circular polarization incident normally on a (001) slab of the crystal. This holds for incidence from either side of the given reciprocal chiral slab since reversing the propagation direction reverses the handedness of the polarization of the plane wave. Therefore we have polarization-selective transmission, where only incident waves with predominant LCP polarization are allowed to pass through.

If we assume that a static uniform magnetic field is applied along the z direction, the scalar Drude permittivity of the plasma spheres becomes a tensor, $\overleftrightarrow{\epsilon_g}$, which has the gyrotropic form given by Eq. (1), where ϵ_r, ϵ_z, and ϵ_κ are given by Eq. (3) with $\tau^{-1} = 0$ since we neglect dissipative losses, and the symmetry of the structure is now described by the nonsymmorphic space group C_4^4 (see the Appendix). In Fig. 4 we depict the calculated photonic band structure in this case, assuming $\omega_c = 0.01\omega_p$. This value of ω_c, though it is by an order of magnitude smaller than that used by Yu *et al.*,[7] for metals corresponds to a prohibitively strong magnetic field, of the order of 10^3 T, but for semiconductors the field becomes much weaker, of the order of 1 T or less. Along the Λ direction, the different bands are labeled by the index of the relevant irreducible representation of the appropriate factor group $\mathcal{G}(\mathbf{k})/\mathcal{T}(\mathbf{k})$ for $\mathbf{k} = (0,0,k_z)$, which is the same as in the absence of a static magnetic field (see Table I). As dictated by group theory, again, the bands along this direction are nondegenerate and the associated Bloch modes are characterized by a different degree of LCP and RCP admixture that varies along a specific band. However, now, since the factor groups which are relevant for the Γ and Z points support only one-dimensional permissible irreducible representations (see Tables IV and V), all degeneracies at these points are removed. For example, as shown in Fig. 4, bands

TABLE IV. Character table of the point group C_4.

	A	B	E_1	E_2
$\widehat{E}$	1	1	1	1
$\widehat{C}_{2z}$	1	1	-1	-1
$\widehat{C}_{4z}$	1	-1	i	$-i$
$\widehat{C}_{4z}^{-1}$	1	-1	$-i$	i

3 and 4 do not cross each other at the Dirac point at the center of the first Brillouin zone and split apart, as anticipated by Yannopapas on the basis of a simple model.[27] However, here, in addition to this splitting, spectral nonreciprocity, $\omega(\mathbf{k}) \neq \omega(-\mathbf{k})$, is also clearly manifested as a result of time-reversal symmetry breaking in conjunction with the lack of space-inversion symmetry. We note that the invariance of Bloch modes that differ by a reciprocal-lattice vector, i.e., here by $(0,0,2\pi n/d), n = 0,\pm1,\pm2,\ldots$, is not violated (see Fig. 4).

In Fig. 4, next to the band diagram, we depict the corresponding transmittance of a (001) slab of the crystal consisting of 16 layers of spheres, for LCP and RCP light incident in (+) and opposite to (−) the direction of the static magnetic field. Though there is no frequency region where only modes with positive or negative group velocity exist, interestingly, in the range from $0.554\omega_p$ to $0.558\omega_p$ we have polarization-selective one-way transmission, where LCP waves are predominantly transmitted in the direction of the static magnetic field while RCP waves are transmitted only

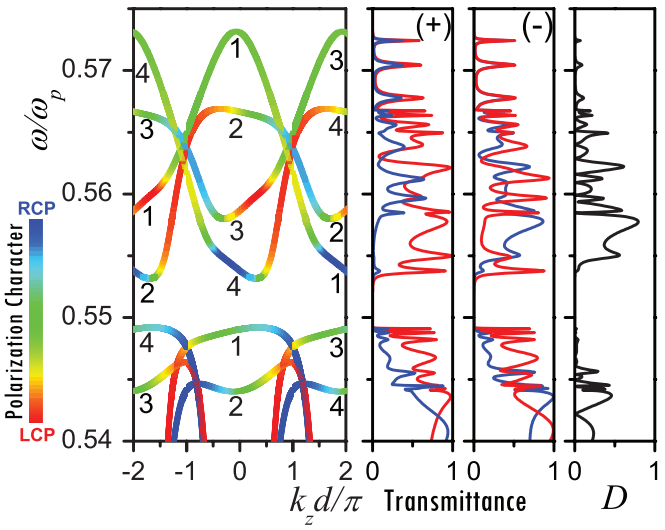

FIG. 4. (Color online) Photonic band structure of the crystal of Fig. 1 along its [001] direction, in a static uniform magnetic field corresponding to $\omega_c = 0.01\omega_p$ applied along the z direction, in the frequency region about the lowest flat bands. The different bands are labeled by the index of the relevant irreducible representation of the appropriate factor group $\mathcal{G}(\mathbf{k})/\mathcal{T}(\mathbf{k})$ for $\mathbf{k} = (0,0,k_z)$ (see Table I). Next to the band diagram we depict the corresponding transmittance of a (001) slab of the crystal consisting of 16 layers of spheres, for LCP and RCP light incident in (+) and opposite to (−) the direction of the static magnetic field. In the right-hand diagram we display the absolute value of the difference between the transmittance in the forward and backward direction, D, which is practically the same for LCP and RCP light.

TABLE V. Characters of the permissible irreducible representations of the factor group $\mathcal{G}(\mathbf{k})/\mathcal{T}(\mathbf{k})$ at the point Z [$\mathbf{k} = (0,0,\pm\pi/d)$] for the space group C_4^4 [$w = \exp(i\pi/4)$].

	Z_1	Z_2	Z_3	Z_4
$\{\widehat{E}\|\mathbf{0}\}\mathcal{T}(\mathbf{k})$	1	1	1	1
$\{\widehat{E}\|4\boldsymbol{\tau}\}\mathcal{T}(\mathbf{k})$	-1	-1	-1	-1
$\{\widehat{C}_{4z}\|\boldsymbol{\tau}\}\mathcal{T}(\mathbf{k})$	w^*	$-w^*$	w	$-w$
$\{\widehat{C}_{4z}\|-3\boldsymbol{\tau}\}\mathcal{T}(\mathbf{k})$	$-w^*$	w^*	$-w$	w
$\{\widehat{C}_{4z}^{-1}\|-\boldsymbol{\tau}\}\mathcal{T}(\mathbf{k})$	w	$-w$	w^*	$-w^*$
$\{\widehat{C}_{4z}^{-1}\|3\boldsymbol{\tau}\}\mathcal{T}(\mathbf{k})$	$-w$	w	$-w^*$	w^*
$\{\widehat{C}_{2z}\|2\boldsymbol{\tau}\}\mathcal{T}(\mathbf{k})$	$-i$	$-i$	i	i
$\{\widehat{C}_{2z}\|-2\boldsymbol{\tau}\}\mathcal{T}(\mathbf{k})$	i	i	$-i$	$-i$

in the opposite direction. The degree of nonreciprocity can be quantified by the absolute value of the difference between the transmittance in the forward and backward direction. This quantity, which vanishes identically if there is no static magnetic field, is displayed in the right-hand diagram of Fig. 4 and is practically the same for LCP and RCP light in the spectral range under consideration. It is worth noting that the frequency regions of increased nonreciprocal response are related to stronger field localization inside the gyrotropic spheres.[42]

V. CONCLUSIONS

In summary, we extended our layer-multiple-scattering method to photonic crystals of gyrotropic spheres using the generalized Mie approach for the evaluation of the single-scatterer T matrix in our spherical-wave basis. By employing this method, we calculated the photonic band structure of a chiral crystal of plasma spheres and corresponding transmission spectra of a finite slab of it, without and under the action of an external static uniform magnetic field. Our results reveal the existence of some intriguing features and effects like Dirac points and polarization-dependent transmission, as well as band splitting and non-reciprocal optical response that stem from time-reversal-symmetry breaking, by virtue of the static magnetic field, in conjunction with the lack of space-inversion symmetry in the crystal. A comprehensive analysis of the results in the light of the theory of nonsymmorphic space groups, which applies to a broader class of photonic crystals that possess nonprimitive translations in their symmetry group, explains consistently all of the observed features and effects to a degree that goes beyond existing interpretation. In this respect, it should be noted that, though there are interesting analogies between electron spin-orbit interaction and optical chirality,[27,43] there is a fundamental difference between electrons, which are spin-one-half fermions, and photons, which are spin-one bosons. For an electron, a rotation by 2π changes the sign of the spin function and the identity operation corresponds to a rotation through 4π, while the polarization vector of a photon remains invariant under a 2π rotation. As a result, the symmetry of electron energy bands in crystalline solids, in the presence of spin-orbit coupling, is described by an appropriate double space group,[44] while for chiral photonic crystals single nonsymmorphic space groups are relevant.

APPENDIX

In this Appendix we apply basic concepts of group theory, and in particular relating to nonsymmorphic space groups, to establish the necessary background for the analysis of symmetry properties of the photonic bands in the structures under study. In general, the symmetry operations that leave a crystal invariant form a group, which is called space group $\mathcal{G}$ of the crystal. A space-group operation, $\{\widehat{P}|\boldsymbol{\tau}_p+\mathbf{R}\}$, transforms a point $\mathbf{r}$ to $\mathbf{Pr}+\boldsymbol{\tau}_p+\mathbf{R}$, where $\mathbf{R}$ is a vector of the underlying Bravais lattice and $\boldsymbol{\tau}_p$ is a nonprimitive translation associated with a (proper or improper) rotation $\widehat{P}$, described by the 3×3 orthogonal matrix $\mathbf{P}$, of the corresponding crystallographic point group $\mathcal{G}_0$. For a symmorphic space group, $\boldsymbol{\tau}_p$ can be taken to be zero for every $\widehat{P}$, which is not the case for a nonsymmorphic space group.

The space group of the crystal of Fig. 1, in the absence of a static magnetic field, is D_4^7.[45] It comprises all combinations of primitive translations of the tetragonal lattice, $\mathbf{R}=n_1\mathbf{a}_1+n_2\mathbf{a}_2+n_3\mathbf{a}_3$, where $\mathbf{a}_1=(a,0,0)$, $\mathbf{a}_2=(0,a,0)$, $\mathbf{a}_3=(0,0,d)$, and $n_1,n_2,n_3=0,\pm1,\ldots$, with the following symmetry operations: $\{\widehat{E}|\mathbf{0}\}$ (identity), $\{\widehat{C}_{2z}|2\boldsymbol{\tau}\}$ (rotation through π about the z axis followed by a translation by $2\boldsymbol{\tau}$), $\{\widehat{C}_{4z}|\boldsymbol{\tau}\}$ (rotation through $\pi/2$ about the z axis followed by a translation by $\boldsymbol{\tau}$), $\{\widehat{C}_{4z}^{-1}|-\boldsymbol{\tau}\}$ (rotation through $-\pi/2$ about the z axis followed by a translation by $-\boldsymbol{\tau}$), $\{\widehat{C}_{2x}|2\boldsymbol{\tau}\}$ (rotation through π about the x axis followed by a translation by $2\boldsymbol{\tau}$), $\{\widehat{C}_{2y}|\mathbf{0}\}$ (rotation through π about the y axis), $\{\widehat{C}_{2a}|\boldsymbol{\tau}\}$ (rotation through π about the [110] axis followed by a translation by $\boldsymbol{\tau}$), and $\{\widehat{C}_{2b}|-\boldsymbol{\tau}\}$ (rotation through π about the $[\bar{1}10]$ axis followed by a translation by $-\boldsymbol{\tau}$), where $\boldsymbol{\tau}=(0,0,d/4)$. Under a static uniform magnetic field along the z direction, the scalar Drude relative electric permittivity of the plasma spheres becomes a tensor, $\overleftrightarrow{\epsilon}_g$, which has the gyrotropic form given by Eq. (1). Therefore only the rotations $\widehat{P}=\widehat{E},\widehat{C}_{2z},\widehat{C}_{4z},\widehat{C}_{4z}^{-1}$ that leave this tensor invariant ($\mathbf{P}\overleftrightarrow{\epsilon}_g\mathbf{P}^{-1}=\overleftrightarrow{\epsilon}_g$) are allowed in the space-group operations, and thus the space group is reduced to C_4^4.[45]

The symmetry of the photonic bands is determined by the group $\mathcal{G}(\mathbf{k})$ of the corresponding wave vector $\mathbf{k}$. This is a subgroup of the space group $\mathcal{G}$ and consists of all transformations $\{\widehat{P}|\boldsymbol{\tau}_p+\mathbf{R}\}$ having the property $\mathbf{Pk}=\mathbf{k}+\mathbf{K}$, where $\mathbf{K}$ is some reciprocal-lattice vector, which may be zero. If we define the group $\mathcal{T}(\mathbf{k})$, which consists of all primitive translations $\{\widehat{E}|\mathbf{R}\}$ that satisfy the equation $\exp(-i\mathbf{k}\cdot\mathbf{R})=1$, $\mathcal{T}(\mathbf{k})$ is obviously a subgroup of the group $\mathcal{T}$ of all primitive translations. Moreover, it is an invariant subgroup of $\mathcal{G}(\mathbf{k})$ and thus it is possible to form the factor group $\mathcal{G}(\mathbf{k})/\mathcal{T}(\mathbf{k})$. In general, the irreducible representations of $\mathcal{G}(\mathbf{k})$ can be obtained from those of $\mathcal{G}(\mathbf{k})/\mathcal{T}(\mathbf{k})$ which satisfy the appropriate conditions, and thus the photonic bands have the symmetry of the permissible irreducible representations of the corresponding factor groups. Though for symmorphic space groups the problem is reduced in finding the irreducible representations of the corresponding point group, $\mathcal{G}_0(\mathbf{k})$, for nonsymmorphic space groups, the factor group is not in general isomorphic to a point group, so that finding its permissible irreducible representations is not straightforward. A method for the construction of character tables for these groups has been proposed by Herring.[46]

The character table of the factor group $\mathcal{G}(\mathbf{k})/\mathcal{T}(\mathbf{k})$ for $\mathbf{k}$ on the axis Λ (see Fig. 1), for both space groups (D_4^7 and C_4^4) which are relevant in this work, is given in Table I. At point Γ ($\mathbf{k}=\mathbf{0}$), the factor group $\mathcal{G}(\mathbf{k})/\mathcal{T}(\mathbf{k})$ is equal to $\mathcal{G}/\mathcal{T}$, which is isomorphic to the point group $\mathcal{G}_0$, i.e., D_4 or C_4 for the D_4^7 or C_4^4 space groups, respectively. The character tables for these point groups are given in Tables II and IV. For point Z, for which $\mathbf{k}=(0,0,\pi/d)$, $\mathcal{T}(\mathbf{k})$ contains all the primitive translations $\{\widehat{E}|n_1\mathbf{a}_1+n_2\mathbf{a}_2+n_3\mathbf{a}_3\}$, except those for which n_1 is an odd integer. The factor group $\mathcal{G}(\mathbf{k})/\mathcal{T}(\mathbf{k})$ contains, therefore, twice as many elements as for Γ. Tables III and V give the character tables of $\mathcal{G}(\mathbf{k})/\mathcal{T}(\mathbf{k})$ for Z, for the D_4^7 and C_4^4 space groups, including only the permissible irreducible representations, i.e., those for which the character for the element $\{\widehat{E}|4\boldsymbol{\tau}\}$ is equal to minus their dimension.

*aristi@ims.demokritos.gr

[1] M. Inoue, R. Fujikawa, A. Baryshev, A. Khanikaev, P. B. Lim, H. Ushida, O. Aktsipetrov, A. Fedyanin, T. Murzina, and A. Granovsky, J. Phys. D: Appl. Phys. **39**, R151 (2006).

[2] B. A. van Tiggelen and G. L. J. A. Rikken, in *Optical Properties of Nanostructured Random Media*, edited by V. M. Shalaev (Springer-Verlag, Berlin, 2002), p. 275.

[3] Z. Wang and S. Fan, Opt. Lett. **30**, 1989 (2005).

[4] K. Fang, Z. Yu, V. Liu, and S. Fan, Opt. Lett. **36**, 4254 (2011).

[5] A. Figotin and I. Vitebsky, Phys. Rev. E **63**, 066609 (2001).

[6] Z. Yu, Z. Wang, and S. Fan, Appl. Phys. Lett. **90**, 121133 (2007).

[7] Z. Yu, G. Veronis, Z. Wang, and S. Fan, Phys. Rev. Lett. **100**, 023902 (2008).

[8] A. B. Khanikaev and M. J. Steel, Opt. Express **17**, 5265 (2009).

[9] A. B. Khanikaev, A. V. Baryshev, M. Inoue, and Y. S. Kivshar, Appl. Phys. Lett. **95**, 011101 (2009).

[10] Y. Hadad and B. Z. Steinberg, Phys. Rev. Lett. **105**, 233904 (2010).

[11] A. B. Khanikaev, S. H. Mousavi, G. Shvets, and Y. S. Kivshar, Phys. Rev. Lett. **105**, 126804 (2010).

[12] F. D. M. Haldane and S. Raghu, Phys. Rev. Lett. **100**, 013904 (2008).

[13] S. Raghu and F. D. M. Haldane, Phys. Rev. A **78**, 033834 (2008).

[14] Z. Wang, Y. D. Chong, J. D. Joannopoulos, and M. Soljačić, Phys. Rev. Lett. **100**, 013905 (2008).

[15] Z. Wang, Y. D. Chong, J. D. Joannopoulos, and M. Soljačić, Nature (London) **461**, 772 (2009).

[16] T. Ochiai and M. Onoda, Phys. Rev. B **80**, 155103 (2009).

[17] X. Ao, Z. Lin, and C. T. Chan, Phys. Rev. B **80**, 033105 (2009).

[18] H. Zhu and C. Jiang, Opt. Express **18**, 6914 (2010).

[19] J. X. Fu, R. J. Liu, and Z. Y. Li, Appl. Phys. Lett. **97**, 041112 (2010).

[20]Y. Poo, R. X. Wu, Z. Lin, Y. Yang, and C. T. Chan, Phys. Rev. Lett. **106**, 093903 (2011).
[21]K. Fang, Z. Yu, and S. Fan, Phys. Rev. B **84**, 075477 (2011).
[22]K. Liu, L. Shen, and S. He, Opt. Lett. **37**, 4110 (2012).
[23]N. Stefanou, V. Yannopapas, and A. Modinos, Comput. Phys. Commun. **113**, 49 (1998).
[24]N. Stefanou, V. Yannopapas, and A. Modinos, Comput. Phys. Commun. **132**, 189 (2000).
[25]V. Karathanos, N. Stefanou, and A. Modinos, J. Mod. Opt. **42**, 619 (1995).
[26]V. Yannopapas, J. Phys.: Condens. Matter **18**, 6883 (2006).
[27]V. Yannopapas, Phys. Rev. B **83**, 113101 (2011).
[28]Y. Zhao, M. A. Belkin, and A. Alú, Nat. Commun. **3**, 870 (2012).
[29]M. Hentschel, M. Schäferling, T. Weiss, N. Liu, and H. Giessen, Nano Lett. **12**, 2542 (2012).
[30]J. Sharma, R. Chhabra, A. Cheng, J. Brownell, Y. Liu, and H. Yan, Science **323**, 112 (2009).
[31]A. Guerrero-Martínez, B. Auguié, J. L. Alonso-Gómez, Z. Džolić, S. Gómez-Graña, M. Žinić, M. M. Cid, and L. M. Liz-Marzán, Angew. Chem., Int. Ed. **50**, 5499 (2011).
[32]X. Shen, C. Song, J. Wang, D. Shi, Z. Wang, N. Liu, and B. Ding, J. Am. Chem. Soc. **134**, 146 (2012).
[33]A. Kuzyk, R. Schreiber, Z. Fan, G. Pardatscher, E. M. Roller, A. Högele, F. C. Simmel, A. O. Govorov, and T. Liedl, Nature (London) **483**, 311 (2012).
[34]N. W. Ashcroft and N. D. Mermin, *Solid State Physics* (Saunders, New York, 1976).
[35]M. Inoue, A. A. Fedyanin, A. V. Baryshev, A. B. Khanikaev, H. Uchida, and A. B. Granovsky, Journal of Magnetics **11**, 195 (2006).
[36]G. W. Ford and S. A. Werner, Phys. Rev. B **18**, 6752 (1978).
[37]Z. Lin and S. T. Chui, Phys. Rev. E **69**, 056614 (2004).
[38]J. L. W. Li and W. L. Ong, IEEE Trans. Antennas Propag. **59**, 3370 (2011).
[39]J. L. W. Li, W. L. Ong, and K. H. R. Zheng, Phys. Rev. E **85**, 036601 (2012).
[40]V. Dmitriev, Eur. Phys. J. Appl. Phys. **32**, 159 (2005).
[41]K. Sakoda, J. Opt. Soc. Am. B **29**, 2770 (2012).
[42]A. B. Khanikaev, A. B. Baryshev, P. B. Lim, H. Uchida, M. Inoue, A. G. Zhdanov, A. A. Fedyanin, A. I. Maydykovskiy, and O. A. Aktsipetrov, Phys. Rev. B **78**, 193102 (2008).
[43]F. Jonsson and C. Flytzanis, Phys. Rev. Lett. **97**, 193903 (2006).
[44]T. Inui, Y. Tanabe, and Y. Onodera, *Group Theory and its Applications in Physics* (Springer, Berlin, 1990).
[45]*International Tables for X-Ray Crystallography*, 5th ed., edited by Th. Hahn, Space Group Symmetry Vol. A (Wiley-VCH, New York, 2005).
[46]C. Herring, J. Franklin Inst. **233**, 525 (1942).